Collapse of DNA under alternating electric fields

Chunda Zhou and Robert Riehn

Phys. Rev. E **92**, 012714 — Published 20 July 2015

DOI: 10.1103/PhysRevE.92.012714

Collapse of DNA under Alternating Electric Fields

Chunda Zhou and Robert Riehn*
Department of Physics, North Carolina State University, Raleigh, NC 27695-8202

Recent studies have shown that double-stranded DNA can collapse in presence of a strong electric field. Here we provide an in-depth study of the collapse of DNA under weak confinement in microchannels as a function of buffer strength, driving frequency, applied electric field strength, and molecule size. We find that the critical electric field at which DNA molecules collapse (10s of kV/cm) is strongly dependent on driving frequency dependent (100 ... 800 Hz) and molecular size (20 ... 160 kbp), and weakly dependent on the ionic strength (8 ... 60 mM). We argue that an apparent stretching at very high electric fields is an artifact of the finite frame time of video microscopy.

PACS numbers: 87.14.gk, 36.20.Ey, 82.35.Lr, 82.35.Rs

I. INTRODUCTION

The mechanical response and dynamics of polyelectrolytes, and particular DNA, is strongly influenced by electric charges and the fields that they create. It thus comes as a surprise that the understanding of the response to strong electric fields is still an active field of research, with a particular interest in the mechanical response to electric field. Initial single-molecule observations reported a stretching along the direction of the a.c. electric field at a few MHz for tethered molecules.[1–3] Simulations of short segments of free polyelectrolytes in electric fields appeared to show the same effect.[4]

Two disparate lines of theory argued for extension of DNA in electric fields, which are based on either the local model of charges coordinated with the polymer backbone (Oosawa-Manning condensed layer or Debye layer), or a meanfield model that treated the polymer as a porous sphere. The local model, which is probably applicable for short DNA molecules, argues for a rod-like description of DNA. As the electric field polarizes the counterions that surround the charged rod molecule, a localized torque is exerted.[5] The local orientation can be detected as an anisotropic conductivity or dichroism of the polyelectrolyte solution.[5, 6] However, how this local order is coupled to a global configuration of a molecule more than a few persistence lengths long in dilute solution is not clear. The meanfield model, which can only be applicable for very large molecules swollen by excluded volume interactions, treats the macromolecule as a semipermeable (ion-selective) sphere with an average density.[7–11] It is implicitly or explicitly assumed that the volume is invariant. Based on these assumptions, and elongation of the of the coil is predicted since an elongated particle has a higher dipole moment (at equal polarization density). The argument certainly is correct for lipid vesicles, where the assumption of constant volume holds.[12]

However, the prediction of extension of polyelectrolytes in an electric field does not appear to hold generally, as a number of recent papers have identified a collapse of DNA and other polyelectrolytes in strong electric fields.[13–17] Collapse can be brought about both by a.c. and d.c. electric fields. Furthermore, a series of prior observations is consistent with the notion that polyelectrolytes should collapse beyond a certain critical electric field strength. For instance, the demonstration of strong aggregation in a solution of small DNA molecules segregates into region of high and very low DNA density suggests that large molecules could also be compacted.[18] Similarly, the aggregation of DNA in strong fields during electroporation was noted.[19]

An understanding of the final state of the collapse transition is emerging. It established that the collapsed state is very dense, indeed dense enough to lead to self-entanglement even of relatively short molecules.[15] The transition is in general marked by hysteresis.[13] The collapse process is gradual, and Wang and Zhu have argued that the diffuse layer must be the leading cause of collapse in poly(2-vinyl pyridine) (P2VP).[16] In comparison, the study of DNA collapse is qualitatively different in that the persistence length of DNA ($\sim 50\,\mathrm{nm}$) is considerably larger than the Debye length ($\sim 3\,\mathrm{nm}$), and so ion transport within one Kuhn segment is clearly differentiated from transport between two such segments.

The driving force the of collapse process is still not fully understood. In an earlier publication that centered on the collapse of nanochannel-confined DNA in a.c. electric fields,[14] we had proposed two possible models. One of the models relied entirely on the motion of ions along the DNA backbone,[20] while the other argues that free ions undergo a concentration polarization in a fashion that is similar to the aggregation process of small DNA molecules.[18] We were not able to distinguish these two clearly.

In the work presented here we conduct a survey of the collapse process under mild confinement as a function of buffer strength, driving frequency, molecule size, and electric field strength. We find a collapse of DNA at critical fields in the range of a few tens of kV/cm, followed by an extension that we attribute to the motion of the molecule in the field of view, and which can be corrected for by using an electrophoretic model. We find a weak

* RRiehn@ncsu.edu

dependence of the critical field for collapse on buffer concentration, and a strong dependence on the size of the DNA coil. Higher frequencies lead to higher threshold field strengths for collapse. We conduct a discussion that considers the different length scales of polarization and conclude that at least the initial contraction must carry a contribution from free ions.

II. EXPERIMENTAL METHODS

We used linearized λ-DNA (48.5 kbp, New England Biolabs) and linearized T4-DNA (∼166 kbp, Nippon Gene), both stained using YOYO-1 (Life Sciences) at a ratio of 1 dye:10 base pairs. We took the fluorescence of YOYO-1 to be the mass density of DNA in our experiment. DNA was dissolved in tris base-boric acid-EDTA (TBE) buffer (pH 8.3) solution with concentrations of 0.25×, 0.5×, 1× and 2×, as well as phosphate-buffered saline (1xPBS) buffer (pH 7.9). 1% β-mercapto ethanol was added in all cases. This leads to ionic strengths of 7.5 mM, 15 mM, 30 mM, 60 mM, and 154 mM, respectively.

YOYO-1 increases the contour length of DNA on the order of 20% for our staining ratio.[21] Günther and coworkers report no significant modification of the persistence length,[22] while others reported a reduction of the persistence length (for instance reduction down to 20% under severe overstaining [23]). We believe that the dye will not modify the qualitative influence of the a.c. electric field.

We fabricated microfluidic fused silica devices by methods described elsewhere.[24] The active region of the device was $650\,nm \times 10\,\mu m \times 500\,\mu m$. The depth of channel is close to the depth of field of the microscope objective we used ($480\,nm$), which is similar to the free radius of gyration of λ-DNA ($\sim 700\,nm$). Platinum wires were inserted into on-chip reservoirs to provide the electric field.

Fluorescence microscopy was performed on an inverted fluorescence microscope (Nikon, TE-2000) with an emCCD camera (Andor, iXon). A 100× oil immersion objective (NA 1.35) was used. Illumination was provided by a 50 mW, 473 nm DPSS laser (Shanghai Dream Lasers) that was controlled through a manufacturer-provided gating input. The intensity of the laser was adjusted by using a neutral density filter. The fluorescence was filtered through a FITC-specific filter set (Semrock). Image frames were taken using strobed illumination.[25] Speckle patterns were blurred by a scanning mirror that is confocal with the back-focal plane of the microscope objective. The angle of incidence is scanned in a 10- or 20-fold zigzag pattern during each frame. Illumination, exposure, and scanning are synchronized through an in-house field-programmable gate array (FPGA) solution.

The same FPGA solution, together with a voltage amplifier (Kepco BOP-1000M), also controls the electric field that is applied to the microchannel through platinum electrodes. The electric field was calculated from the potential difference detected in a four-point probe setup that had two electrodes in each reservoir. Small, random offsets of amplifier and electrode asymmetry are canceled by control based on proportional-integral-differential (PID) feedback from the real-time image detected by the camera.

For each DNA molecule, a 30- to 45-second video containing several hundred frames was taken. Based upon the individual frames of each video, the time evolution of the radius of gyration, R_g, as well as a shape numeric measure for the shape anisotropy were calculated. Both values are based on the gyration tensor S_{mn}. S_{mn} is of size 2×2 with m and n chosen from $\{x, y\}$. For an image with the intensity matrix I_{ij}, the S_{mn} can be expressed as

$$S_{mn} = \frac{1}{\sum_{(i,j)\in\mathbb{A}} I_{mn}} \sum_{(i,j)\in\mathbb{A}} I_{ij} {r_m}^{(j)} {r_n}^{(i)} \qquad (1)$$

where $r_m^{(i)}$ is the position of the i^{th} pixel along the m-coordinate in center of mass coordinate frame. S_{mn} is a symmetric positive definite matrix. Thus the sum of the squares of the eigenvalues of S (λ_x and λ_y) is R_g^2.[26] The shape isotropy can be quantified by $\frac{|{\lambda_x}^2 - {\lambda_y}^2|}{{R_g}^2}$.

Both R_g and anisotropy were first averaged over all frames of a video belonging to a single molecule, and the weighted average over multiple molecules was formed for each condition. We determine the error of the mean of the variable x by [27]

$$\sigma = \sqrt{\frac{1}{\sum_a n_a - 1}\left(\sum_a (n_a - 1)\sigma_a + \sum_a n_a(\bar{x}_a - \bar{x})^2\right)} \qquad (2)$$

where n_a is the number of data points within molecule a, σ_a is the variance within molecule a, $\bar{x}_a$ is the mean for molecule a, and $\bar{x}$ is the weighted average over all molecules.

III. EXPERIMENTAL RESULTS

Each molecule was brought individually into the field of view, and the electric field strength was varied while observing the same molecule. Fig. 1 shows time-lapse micrographs of the response of the molecule to the electric field in 1× TBE. The field runs top to bottom in these images, and oscillates at 300 Hz. At low electric fields the molecule had an asymmetric typical random-walk shape and fluctuated (Fig. 1A).[28] As the electric field was raised to a few tens of kV/m, the size of of the molecule decreased while the apparent fluctuations were retained (Fig. 1B at 24 kV/m). In particular, frames with very compact molecule configurations occurred with increasing frequency. At sufficiently high fields, only extremely compact and round configurations were observed (Fig. 1C at 66 kV/m). When the field was further increased, the molecule appeared to elongate in the direction of the electric field (Fig. 1D at 122 kV/m).

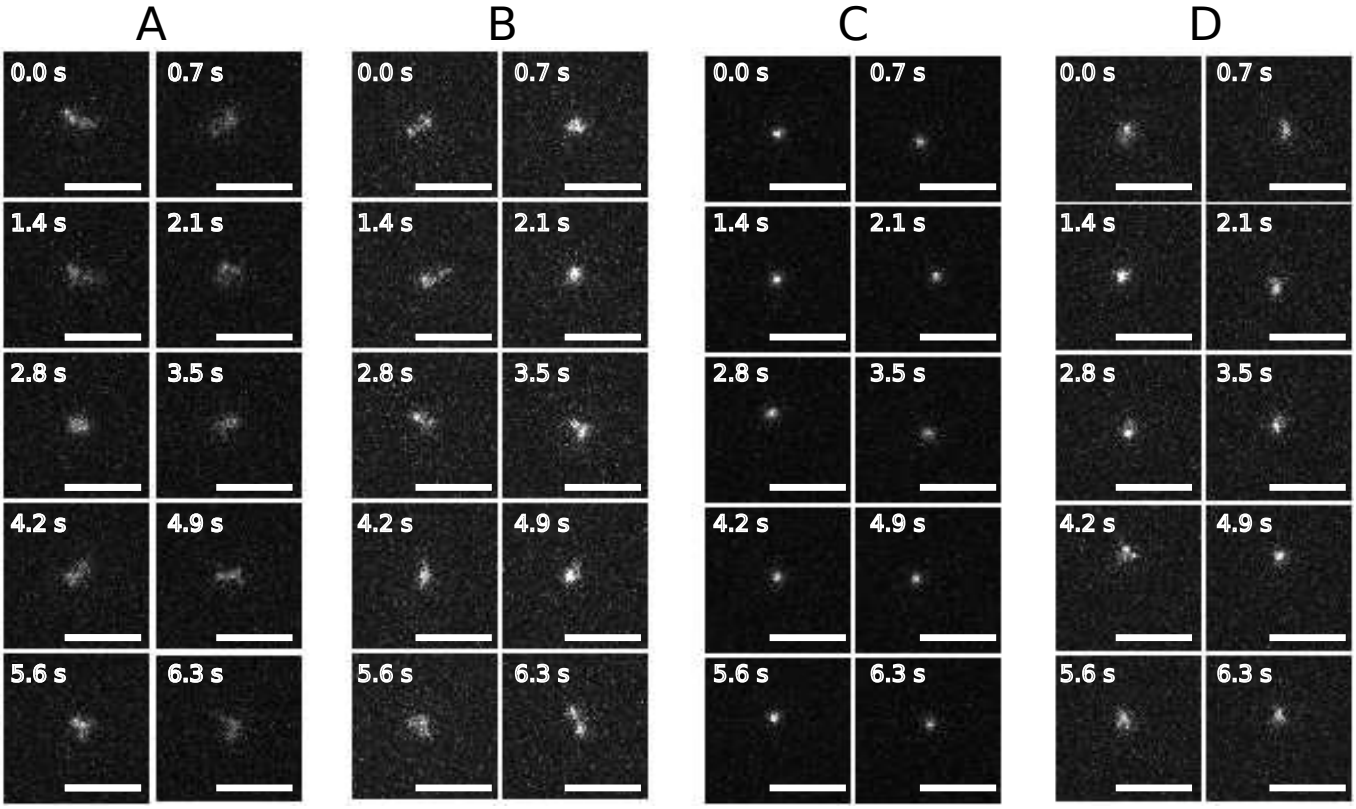

FIG. 1. Images of λ-DNA in alternating electric fields at 300 Hz in 1x TBE. (A) 0 kV/m, (B) 24 kV/m, (C) 66 kV/m, (D) 122 kV/m. The scale bar is 5 microns.

The collapse was observed under all conditions that we attempted. In particular, we tested devices with a depth between 0.25 and 1.0 micrometer. Collapse was observed both in the weakly dissociated TBE buffer as well as in the strongly dissociated 1×PBS buffer. Finally, we investigated whether turbulent flows due to electroendosmosis could be the source of the collapse. To that end we added 0.5% by weight of either polyvinylpyrrolidone (PVP, 350 kDa) or linear polyacrylamide (POP6, proprietary mixture of ABI). The collapse was observed in both cases.

Thus we concluded that the applied field strength, the field frequency, the ionic strength, the charge of the molecule, and the molecule size were the most likely factors in the collapse. We have no meaningful approach to independently influence the linear charge density of DNA. The other parameters were varied over a practical range.

We analyzed videos of this kind for λ-DNA in 0.25×, 0.5×, 1.0×, and 2.0× TBE at six a.c. frequencies between 100 Hz and 800 Hz and a field strength up to 150 kV/m. Multiple DNA molecules were observed independently at the same condition, and clearly broken molecules with a field-free R_g different than that commonly observed at the respective buffer concentration were rejected. Molecules for which the feed-back stabilization of the position in the field of view failed could also not be utilized.

In Fig. 2 we present R_g and anisotropy for 2× TBE and 300 Hz for four molecules after averaging over all frames for each individual molecule, but before averaging over multiple molecules. Fig. 2A shows R_g, one of which is apparently smaller than the others and may be a sheared molecule. R_g for each molecule undergoes a collapse when the electric field strength increased from 0 kV/m to about 130 kV/m. Beyond that point, the radius of gyration appeared to increase in an almost linear fashion.

In Fig. 2B we show that the anisotropy gradually decreased as R_g approached its minimum. Beyond the minimum in R_g, the anisotropy strongly increased. We also tracked the mean orientation of the molecule under collapse which is given by the eigenvector belonging to the largest eigenvalue of S_{mn} (not shown), but did not find an alignment of the molecule as it approached the point of maximum collapse. After the point of highest collapse, the orientation was along the electric field direction.

Fig. 3A-D shows the experimentally observed R_g for all salt strengths and driving frequencies for λ-DNA in TBE. The collapse was observed under all buffer conditions used. We also systematically found that the collapse appears to be strongly dependent on the excitation frequency. In particular, the point of maximum contraction and the amount of contraction appeared to shift. Additionally, the slope of the linear part of the curve at

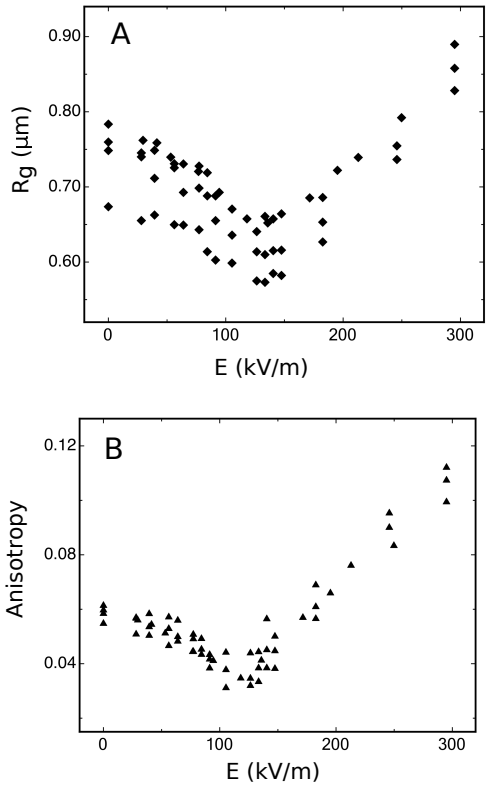

FIG. 2. (A) Radius of gyration changes with electric field strength in 2×TBE and 300 Hz electric field. Each black square at constant electric field strength represents a molecule. (B) Anisotropy as function of strength in 2×TBE and 300 Hz electric field. Each black triangle at constant electric field strength represents a molecule.

high field appears to be dependent on the driving frequency.

This linear rise could either be due to a real stretching, as traditionally assumed, or it could be due to a sinusoidal center of mass motion of the molecule because the time per frame covers multiple a.c. periods. For real stretching of the molecule we would expect a saturation of R_g at $L/\sqrt{24}$, where L is the fixed contour length. We would also expect a symmetric brightness distribution along the axis of molecule elongation. Since neither is generally observed, we conclude that a center of mass motion is the cause.

If the time per frame is an integer multiple of the oscillation period and we assume that the DNA is described by the motion of a fully collapsed point particle, we anticipate that the intensity $I(x)$ along the axis of the channel has the form $I(x) \propto \left((\Delta x/2)^2 - x^2\right)^{-1/2}$ with $x \in [-\Delta x/2, \Delta x/2]$. For a fixed mobility $\Delta x \propto \mu E/f$, where μ is the salt-dependent mobility. A 2-dimensional image can be predicted by describing DNA and optics by a Gaussian point spread function (PSF). In Fig. 4 we show good agreement between experiment and this calculation.

We can now estimate the effect of this motion on the experimentally observed radius of gyration, $R_{g,\mathrm{expt}}$, as $R_{g,\mathrm{expt}} = \sqrt{R_{g,\mathrm{phys}}^2 + (\alpha\Delta x)^2}$ where $R_{g,\mathrm{phys}}$ is the physical (real) radius of gyration, α is a shape factor that is constant, and Δx indicates the maximum periodic displacement. For each curve in Fig. 3A-D we thus applied the correction

$$R_{g,\mathrm{phys}}^2 = \sqrt{R_{g,\mathrm{expt}}^2 - (\gamma E)^2} \tag{3}$$

to obtain Fig. 3E-H by determining a unique γ value for each pair of buffer strength and driving frequency so that $R_{g,\mathrm{phys}}$ assumed a constant value at high electric fields. It appears that collapse is achieved at all salt strength and frequencies. No error for the γ determination can be explicitly given since this would require a functional form to perform a full numerical fit, which we do not have.

By following the argument above, we identify $\gamma = \frac{\alpha\mu}{f}$. For 0.5×TBE and 2×TBE, γ followed a $1/f$ relationship as anticipated (Fig. 5A). The other two are not shown since for 0.25×TBE, it appeared that the minimum R_g was not reached for all frequencies, and the graph for 1×TBE appears to contain electroosmotic instabilities of liquid movement in the channel at some frequencies. While we do not quantify α, it is interesting to note that $\mu \approx 10^{-4}\, cm^2/V\cdot s$, on the order of the free-solution mobility of DNA, and that lower salt leads to higher mobility, as anticipated.[29] However, the apparent mobility could also carry an electroendosmotic contribution that we cannot detect because we are phase-insensitive.

The functional form of the correction factor further predicts that the zero-intercept of a linear fit to the linear region of the R_g *vs.* $|E|$ graphs (Fig. 3A-D) yields $R_{g,\mathrm{phys}}$ in the limit of very high electric fields. For experiments with λ-DNA in 0.5×TBE, 1×TBE and 2×TBE, we observed a minimum radius that is ≈400 nm, while for 0.25×TBE we recorded ≈560 nm. The radius of gyration of an optical PSF with width σ in two dimensions is $\sqrt{2}\sigma$, which for our objective and emission wavelength is 360 nm. We thus believe that the apparent size of DNA is limited by the diffraction. Further removal of the influence of diffraction yields a value in the order of 200 nm to 400 nm, but with very high uncertainty.

The combination of the linear behavior at high electric fields, the correct frequency dependence, and the observation that the intercept of the linear fit gives a physically meaningful value makes us confident that the blurring due to a center of mass motion is the likely cause of the linear rise of R_g at high electric fields.

In order to gain an understanding of the physics of the collapse process, a critical electric field strength E_c was defined and evaluated. Because we currently lack a model for the process, it is chosen as the electric field of the half way point of the collapse of an individual $R_{g,\mathrm{phys}}$ curve. We show $E_c(f)$ for λ-DNA in TBE in Fig. 5. E_c was approximately proportional to f, although the error introduced in the pathway of high-field drift correction and E_c determination certainly introduces a considerable

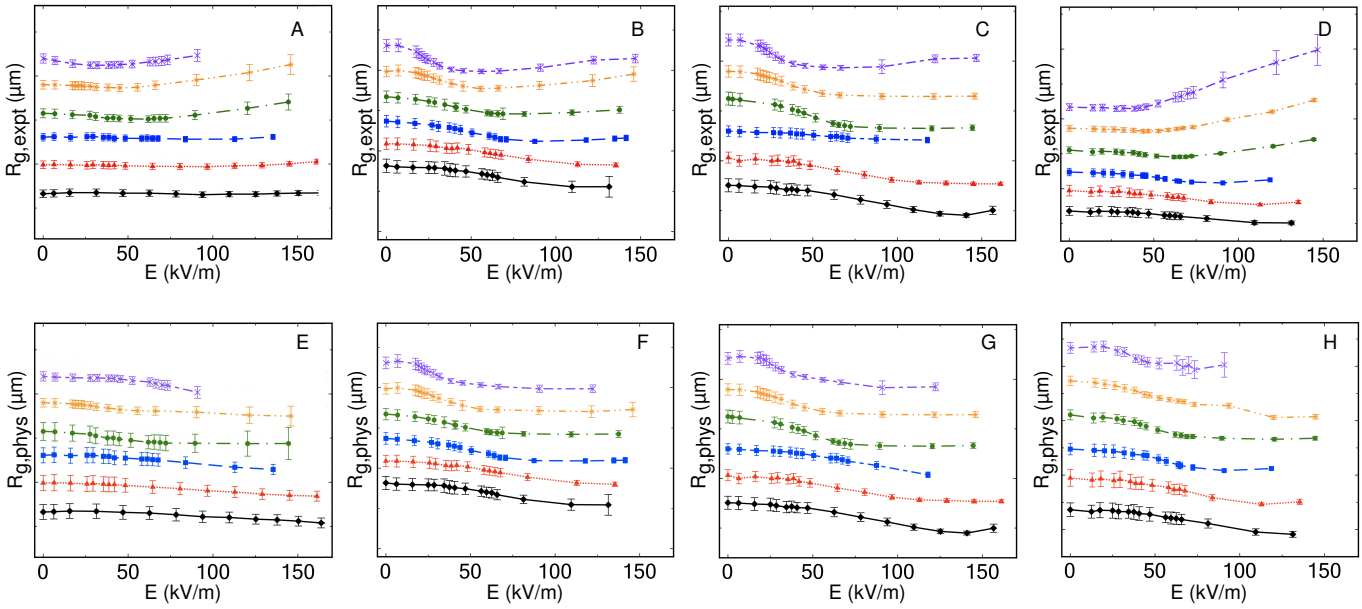

FIG. 3. Radius of gyration of λ-DNA as function of salt strength and frequency. We show the experimentally measured radius of gyration $R_{g,\mathrm{expt}}$ in panels (A-D) ((A) 0.25×TBE, (B) 0.5×TBE, (C) 1×TBE, (D) 2×TBE). The physical radius of gyration $R_{g,\mathrm{phys}}$ recovered after correction of motion during each video frame is shown in panels (E-F) ((E) 0.25×TBE, (F) 0.5×TBE, (G) 1×TBE, (H) 2×TBE). Curves for different frequencies are separated by a 0.3 μm offset (Purple × - 100 Hz, yellow ∗ - 200 Hz, green ◯ - 300 Hz, blue □ -450 Hz, red △ - 675 Hz, black ◊ - 800 Hz).

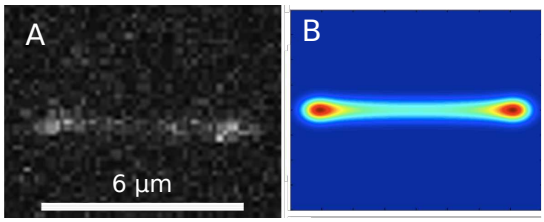

FIG. 4. Image pattern due to center of mass motion. (A) is a typical image in experiments (λ-DNA in 2×TBE and 146.82 kV/m, 100 Hz driving). (B) is a simulation of a molecule under sinusoidal motion and extended illumination.

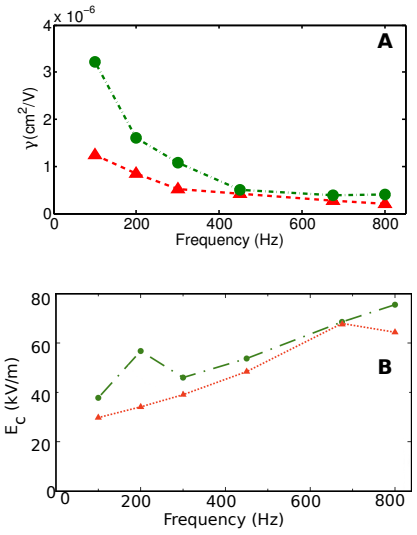

FIG. 5. (A) Correction factor γ as function of driving frequency. (Green ◯ - 2×TBE, red △ - 0.5×TBE). No error bars given as fit was performed manually. (B) Critical electric field strength *vs.* electric field frequencies (same color coding).

error. We thus cannot exclude that a non-linear relationship. We did not observe a salt concentration dependence beyond the statistical uncertainty in Fig. 5.

For comparison, we also calculated E_c for our previously published dataset on DNA collapse in nanochannels E_c (Fig. 6) did not contain such a strong signature of the high-electric field drift. [14] This is because R_g along the channel axis is far larger than the center of mass movement. In that case, we find a convex curve for narrow channels. While for wider channels both a linear or a convex relationship between E_c and the driving frequency are possible. Note that the curved/linear transition could be due to differences in large-scale charge distribution and hydrodynamic coupling.

In order to investigate the influence of spatial extent of the molecule, we repeated the experiment using a mixture of T4-DNA, its fragments, and its multimers in 2×TBE at 300 Hz driving frequency (Fig. 7). We categorized molecules into four groups (short, medium, long and extremely long) based on the zero-electric-field $R_{g,\mathrm{expt}}$ after indiscriminately recording all molecules. Fig. 7A shows the resulting $R_{g,\mathrm{expt}}(E)$. All groups share the same high-field linear asymptotic curve, which is consistent with the hypothesis that this region is dominated by a drift of

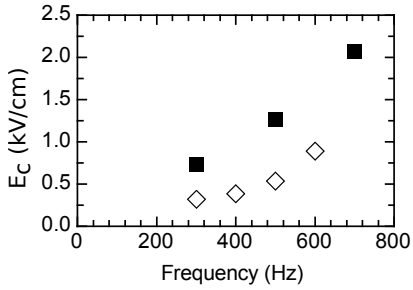

FIG. 6. Critical electric field strength *vs.* electric field frequencies for λ-DNA in nanochannels.[14] The solid square curve is the result from $225 \times 325\,nm^2$ channels. The empty square curve is the result from $80 \times 100\,nm^2$ channels.

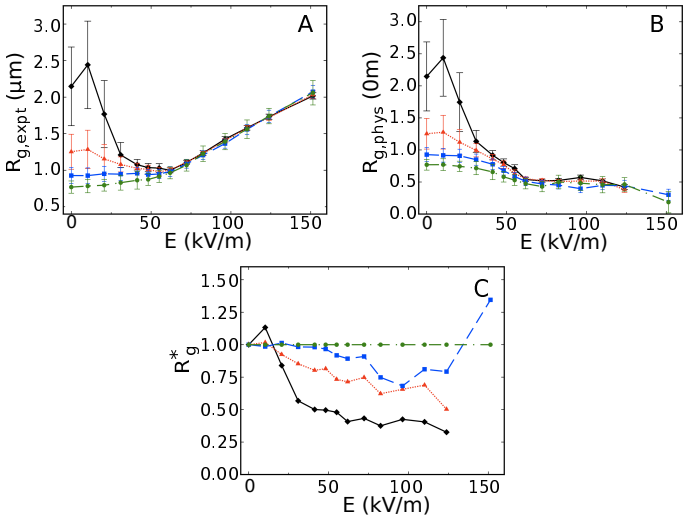

FIG. 7. Radius of gyration of T4-DNA multimers and fragments as function of electric field strength in 2×TBE at 300Hz driving frequency. Probable length assignment: black ◊ - double T4 (∼ 320 kbp), red △ - single T4 (∼ 160 kbp), blue □ - half T4 (∼ 80 bp), green ◯ - quarter T4 (∼ 40 kbp), (B) Radius of gyration of T4-DNA multimers and fragments as function of electric field strength in 2×TBE at 300 Hz driving frequency, after correction for the center of mass motion. (C) Normalized relative radius of gyration of T4-DNA in 2× TBE (see text for definition).

the center of mass of the molecule with a mobility that is independent of molecular weight. Intriguingly, we observed an apparent expansion of the largest two molecule groups at low electric field strengths, but warn about its limited statistical weight. Fig. 7B shows $R_{g,\mathrm{phys}}(E)$ after the center of mass drift correction and indicates collapse for all four groups. Using the same extrapolation procedure as above, we find that the two largest groups did not quite achieve the diffraction-limited radius but contracted to $R_g \approx 500 - 600\,\mathrm{nm}$, while the two smaller groups again collapsed to a diffraction-limited size. Because large molecules were much larger initially, that means that the larger molecules contracted to a smaller fraction upon application of the a.c. field.

Since the degrees of collapse were considerably different between different lengths, and thus visual comparison is difficult, we plotted the parameter

$$R_g^* = \frac{R_{g,\mathrm{phys}}^{\mathrm{small}}\left(0\frac{V}{m}\right) R_{g,\mathrm{phys}}^{(i)}(E)}{R_{g,\mathrm{phys}}^{(\mathrm{i})}\left(0\frac{V}{m}\right) R_{g,\mathrm{phys}}^{\mathrm{small}}(E)}$$

where $R_{g,\mathrm{phys}}^{\mathrm{small}}$ is for the smallest group (which we presume to have the least collapse), and $R_{g,\mathrm{phys}}^{(i)}$ is for group (i). A value of 1 denotes thus a relative collapse on par with the smallest series, and below a stronger collapse. In Fig. 7C we observe that larger molecules not only collapse to a greater degree, but that this greater degree of collapse is obtained at lower E the larger the molecule is.

IV. DISCUSSION

It is self-evident that co- and counterion concentration polarization are linked to the collapse. Dielectric impedance spectroscopy suggests a set of distinctive length-scales.[30–32] We will discuss the likely leading cause of collapse in terms of these length-scales and the the likely mode of polarization. Without specifying the specific nature of the polarized ion (Oosawa-Manning-condensed, Debye-layer or free) we can define a polarization length scale that is the distance over which ions can diffuse during a single oscillation period of the electric field. The polarization scale of the Tris-H^+ ion is

$$\lambda_\omega = \sqrt{\frac{D}{\omega}}\ , \tag{4}$$

were D is the diffusion coefficient. The collapse must be an in-phase phenomenon as lower frequencies decrease the critical field strength (Figs. 5&6), and Doyles group reported collapse in a d.c. field.[15] For free counterions, D is the free-solution diffusion coefficient of Tris-H^+, which we determined from the limiting conductance of Tris·HCl solution.[33] For a 500 Hz driving electric field, this polarization scale is ∼500 nm.

We first consider ion motion over the length-scale of a persistence length or shorter. In the bound ion model,[34–36] counterions move along the polymer backbone until they either encounter the end of a DNA strand or a bent region where the curvature vector is parallel or antiparallel to the electric field.[14, 20, 37] At these points charges collect. For strands of opposing curvature vector, the induced charges are of opposite polarity. As a result, we proposed that neighboring segments of opposing curvature attract each other, leading to an collapse effect. A detailed model considers the influence of the induced charge density on the local curvature.[20]

While the model is likely to contribute to the collapse once high densities are reached, we believe that it is not complete, and that another mechanism is needed at least in the early stages. Firstly, in λ-DNA very few chain-chain contacts exist,[38, 39] and only few of those

contacts will be correctly oriented. Further, the frequency range between a few 100 Hz to 1 kHz (Figs. 5&6) does not overlap with the "high-frequency" resonant feature at a few MHz in dielectric spectroscopy[32, 40] because persistence length (~ 50 nm) and Debye length ($\sim 0.7 \ldots 3.6$ nm) are far smaller[30, 34–36, 41–44] the a relaxation length scale at 500 Hz unless condensed ions have very different dynamics than free ions.[45–48]

We therefor believe that relaxation of non-condensed ions on scales of many persistence lengths causes the collapse. The compaction can proceed either through a meanfield effect that exerts pressure on the entire molecule, or through an interaction of polarizable subunits. We will briefly discuss both scenarios. A meanfield effect is based on large-scale disturbance of the ion concentrations within and neighboring to the molecule. This could occur at large electric fields if ions are stripped off the backbone of DNA and subsequently exchanged with buffer ions. [49–53] In particular, the Musheev et al. report collapse due to stripping of all condensed ions.[54] This is in analogy with the Wien effect, a field-dependent dissociation of counterions.[55] Effects either reminscent of this effect, or directly attributed to it, have been reported in experiments at similar fields, time scales, and molecular weights to ours. [56–59] Fischer and Netz identified a "ulta-low-frequency" relaxation mode for polyelectrolytes due to transfer of charges between strands.[44] A second source of mean-field pressures is a concentration polarization of the co- and counter ions around the entire molecules in high fields that has been considered by a number of groups.[10, 60, 61] The critical field-frequency relationship arises within the meanfield assumption because decreasing driving frequency enables the full polarization of increasingly larger polymer coils. Interestingly, the weak ionic strength dependence found here mirrors the weak dependence of the voltage threshold of the limiting current in ion-selective membranes.[62] Viovy's group used the effect of the pressure due ion concentration polarization to explain the aggregation of DNA molecules under an a.c. electric field.[18, 63, 64] In particular, Mitnik et al. find a critical electric field-frequency relationship similar to ours. Concentration polarization at the end of DNA in nanochannels has been predicted.[65]

Collapse due to interacting subunits requires inhomogeneities of the polarization density. The counterion density without electric field roughly follows that of the polymer backbone which its fluctuates.[66] We propose that the combination of counterion cloud displacement relative to the polymer backbone in an electric field and thermal polymer density fluctuations leads to a fluctuating polarization density. Dipole moments of neighboring dense polymer regions will be oriented in the same direction, and thus subunits attract.[11] One could object to the notion of polarized subunits on the grounds that Oosawa-Manning condensation localizes polarization close to DNA. However, the field strength is likely high enough to induce Wien effect and the scale of the double-layer is strongly modified by the electric field.[67] Furthermore, concentration polarization for individual subunits could become applicable, and would lead to localized dipoles of subunits within the polymer.[10, 11, 60] The frequency dependence arises from the largest subunit that can be effectively polarized by the driving frequency.

If polarizable subunits are the cause of collapse, then we also have to consider hydrodynamic interactions between those units, analogous to microspheres in a.c. fields. There, chaining is expected in absence of hydrodynamic interactions.[68] However, aggregation is observed,[69] and good agreement between experiment and models that contain both ion polarization and hydrodynamic coupling was achieved.[63, 70] While hydrodynamic interactions may have an influence in microchannels and free solution, the presence of collapse in nanochannels[14] is strong indication that they are not the leading cause. In nanochannels, Brochard and de Gennes argued that hydrodynamic interactions are screened on a length scale similar to the channel diameter.[71] Furthermore, Bakajin et al. found that hydrodynamic interactions break down in nanoslits shallower than 100 nm.[72] However, the different shapes Figs. 5&6 may point to a possible subtle difference in the way that hydrodynamic coupling acts for micro-and nano-confinement (Figs. 5&6). We do not believe that the properties of the channel walls (such as patches of different electrosmosis) are responsible for the collapse, since the results are very robust over a wide range of channel geometries.

Both hypotheses based on scales beyond the persistence length (mean-field, interacting subunits) are consistent with Fig. 7. If the collapse is based on polarizable subunits, then we expect that larger molecules have more subunits in the correct relative position for attractive interaction, especially if the number of subunits is $\mathcal{O}(1)$. On the other hand a compression by a concentration polarization outside of the molecule is also plausible as a larger molecule presents an ion-selective barrier that is longer and has fewer "holes" created by density fluctuations.

The minimum collapse R_g or λ-DNA (after removal of center of mass motion and optical PSF) potentially differentiates the two mechanisms bad on large-scale polarization: it is on the order of 200 nm to 400 nm at 0.5×TBE, on the order of a single units given by the free-ion relaxation scale that was identified earlier (especially at low frequencies). Thus, the coil could not be comprised of multiple polarizable subunits, but would appear as one single unit. Thus only the "meanfield" interpretation would appear possible. However, it is conceivable that the initial collapse occurs through an interaction of subunits, and that curvature-dependent local polarization at the length scale of a persistence length takes over as the driving force of the ultimate collapse R_g. The contour-length dependence of the minimum collapse radius (Fig. 7) indicates that the radius is likely not limited by a polarization length scale, but rather by the

local pressure within the coil.

V. CONCLUSIONS

We have demonstrated DNA collapse in an a.c. electric field in dilute solution under weak confinement. We have explored the tunable parameters accessible to us to understand the collapse process, and found a contraction under all conditions. From the combination of frequency dependence, influence of molecular weight, and relatively insensitivity to ionic strength, we believe that a polarization of ions beyond the Debye and Oosawa-Manning condensed layers is responsible for collapse.

Our work points to a number of unresolved questions, and a particular the need to find numerical methods to investigate all processes of the system self-consistently. The large range of length-scales native to the problem, from the extent of an ion in the condensed layer to the extent of a whole molecule with up to 10^6 base pairs, is the primary challenge. The specific questions are the possibility of a local Wien effect in presence of condensed ions, the larger scale ion polarization pattern around the polymer backbone, and how ion clouds are deformed on large scales to form a polarization pattern on the order of micrometers. The work also points towards the poor understanding of the range over which linear electrodiffusion assumptions hold.

ACKNOWLEDGMENTS

We thank Robijn Bruinsma for discussions. We acknowledge support from the National Institutes of Health (R21HG004383, R21CA132075). Part of this work was performed in part at CNF, supported by NSF (ECS-0335765).

[1] M. Washizu and O. Kurosawa, IEEE Transactions on Industry Applications **26**, 1165 (1990).
[2] S. Suzuki, T. Yamanashi, S. Tazawa, O. Kurosawa, and M. Washizu, IEEE Transactions on Industry Applications **34**, 75 (1998).
[3] C. Wälti, P. Tosch, A. G. Davies, W. A. Germishuizen, and C. F. Kaminski, Applied Physics Letters **88**, 3 (2006).
[4] H. Liu, Y. Zhu, and E. J. Maginn, Macromolecules **43**, 4805 (2010).
[5] M. Eigen and G. Schwarz, Journal of Colloid Science **12**, 181 (1957).
[6] C. Houssier and E. Fredericq, Biochimica et Biophysica Acta **88**, 450 (1964).
[7] J. J. Hermans, Journal of Polymer Science **18**, 527 (1955).
[8] J. T. G. Overbeek and D. Stigter, Recueil des Travaux Chimiques des Pays-Bas **75**, 543 (1956).
[9] F. Oosawa, *Polyelectrolytes* (Marcel Dekker, New York, 1971).
[10] M. Fixman and S. Jagannathan, Macromolecules **16**, 685 (1983).
[11] A. Cebers and I. Rubinstein, International Journal of Modern Physics B **16**, 2334 (2002).
[12] M. Winterhalter and W. Helfrich, Journal of Colloid and Interface Science **122**, 583 (1988).
[13] S. Wang, H.-C. Chang, and Y. Zhu, Macromolecules **43**, 7402 (2010).
[14] C. Zhou, W. W. Reisner, R. J. Staunton, A. Ashan, R. H. Austin, and R. Riehn, Physical Review Letters **106**, 248103 (2011).
[15] J. Tang, N. Du, and P. S. Doyle, Proceedings of the National Academy of Sciences of the United States of America **108**, 16153 (2011).
[16] S. Wang and Y. Zhu, Biomicrofluidics **6**, 24116 (2012).
[17] C.-h. Lee and C.-c. Hsieh, Biomicrofluidics **7**, 14109 (2013).
[18] L. Mitnik, C. Heller, J. Prost, and J.-L. Viovy, Science **267**, 219 (1995).
[19] A. G. Sabelnikov and E. S. Cymbalyuk, Bioelectrochemistry and Bioenergetics **24**, 313 (1990).
[20] R. F. Bruinsma and R. Riehn, Chemphyschem **10**, 2871 (2009).
[21] T. T. Perkins, D. E. Smith, R. G. Larson, and S. Chu, Science **268**, 83 (1995).
[22] K. Günther, M. Mertig, and R. Seidel, Nucleic Acids Research **38**, 6526 (2010).
[23] A. Sischka, K. Toensing, R. Eckel, S. D. Wilking, N. Sewald, R. Ros, and D. Anselmetti, Biophysical Journal **88**, 404 (2005).
[24] R. Riehn, R. H. Austin, and J. C. Sturm, Nano Letters **6**, 1973 (2006).
[25] A. Karpusenko, J. H. Carpenter, C. Zhou, S. F. Lim, J. Pan, and R. Riehn, Journal of Applied Physics **111**, 24701 (2012).
[26] D. N. Theodorou and U. W. Suter, Macromolecules **18**, 1206 (1985).
[27] J. R. Turner and J. F. Thayer, *Introduction to Analysis of Variance: Design, Analyis & Interpretation* (SAGE Publications, Thousand Oaks, CA, 2001).
[28] C. Haber, S. A. Ruiz, and D. Wirtz, Proceedings of the National Academy of Sciences of the United States of America **97**, 10792 (2000).
[29] D. A. Hoagland, E. Arvanitidou, and C. Welch, Macromolecules **32**, 6180 (1999).
[30] F. Bordi, C. Cametti, and R. H. Colby, Journal of Physics: Condensed Matter **16**, R1423 (2004).
[31] A. Bonincontro, C. Cametti, A. Di Biasio, and F. Pedone, Biophysical Journal **45**, 495 (1984).
[32] S. Tomić, S. Dolanski Babić, T. Vuletić, S. Krča, D. Ivanković, L. Griparić, and R. Podgornik, Physical Review E **75**, 021905 (2007).
[33] S. D. Klein and R. G. Bates, Journal of Solution Chemistry **9**, 289 (1980).
[34] J. P. McTague and J. H. Gibbs, Journal of Chemical Physics **44**, 4295 (1966).
[35] F. Oosawa, Biopolymers **9**, 677 (1970).
[36] F. van der Touw and M. Mandel, Biophysical Chemistry

2, 218 (1974).
[37] D. Pörschke, E. R. Schmidt, T. Hankeln, G. Nolte, and J. Antosiewicz, Biophysical Chemistry **47**, 179 (1993).
[38] R. M. Robertson, S. Laib, and D. E. Smith, Proceedings of the National Academy of Sciences of the United States of America **103**, 7310 (2006).
[39] D. R. Tree, A. Muralidhar, P. S. Doyle, and K. D. Dorfman, Macromolecules **46** (2013), 10.1021/ma401507f.
[40] D. J. Bakewell, I. Ermolina, H. Morgan, J. Milner, and Y. Feldman, Biochimica et Biophysica Acta **1493**, 151 (2000).
[41] S. S. Dukhin and V. N. Shilov, *Dielectric Phenomena and the Double Layer in Disperse Systems and Polyelectrolytes* (John Wiley & Sons Inc, New York, 1974).
[42] M. Fixman, Macromolecules **13**, 711 (1980).
[43] W. Van Dijk, F. Van Der Touw, and M. Mandel, Macromolecules **14**, 792 (1981).
[44] S. Fischer and R. R. Netz, European Physical Journal E **36**, 117 (2013).
[45] W. K. Kim and W. Sung, Physical Review E **78**, 021904 (2008).
[46] T. E. Angelini, R. Golestanian, R. H. Coridan, J. C. Butler, A. Beraud, M. Krisch, H. Sinn, K. S. Schweizer, and G. C. L. Wong, Proceedings of the National Academy of Sciences of the United States of America **103**, 7962 (2006).
[47] B. I. Shklovskii, Physical Review Letters **82**, 3268 (1999).
[48] S. Fischer, A. Naji, and R. R. Netz, Physical Review Letters **101**, 176103 (2008).
[49] S. Frank and R. G. Winkler, Europhysics Letters **83**, 38004 (2008).
[50] X. Schlagberger and R. R. Netz, Europhysics Letters **83**, 36003 (2008).
[51] F. Bailey, A. P. Jr, and R. Fuoss, Journal of the American Chemical Society **2636**, 4 (1952).
[52] G. S. Manning, Biophysical Chemistry **9**, 189 (1977).
[53] M. Nagasawa, I. Noda, T. Takahashi, and N. Shimamoto, Journal of Physical Chemistry **76**, 2286 (1972).
[54] M. U. Musheev, M. Kanoatov, C. Retif, and S. N. Krylov, Analytical Chemistry **85**, 10004 (2013).
[55] L. Onsager and S. K. Kim, Journal of Physical Chemistry **61**, 198 (1957).
[56] D. Pörschke, Biopolymers **15**, 1917 (1976).
[57] S. Diekmann and D. Pörschke, Biophysical Chemistry **16**, 261 (1982).
[58] D. Pörschke, Biophysical Chemistry **22**, 237 (1985).
[59] M. Jonsson, U. Jacobsson, M. Takahashi, and B. Nordén, Journal of the Chemical Society, Faraday Transactions **89**, 2791 (1993).
[60] P. P. Gopmandal and S. Bhattacharyya, Colloid and Polymer Science **292**, 905 (2013).
[61] H.-P. Hsu and E. Lee, Journal of colloid and interface science **390**, 85 (2013).
[62] I. Rubinstein and L. Shtilman, Journal of the Chemical Society, Faraday Transactions 2 **75**, 231 (1979).
[63] H. Isambert, A. Ajdari, J.-L. Viovy, and J. Prost, Physical Review E **56**, 5688 (1997).
[64] S. Magnúsdóttir, H. Isambert, C. Heller, and J.-L. Viovy, Biopolymers **49**, 385 (1999).
[65] S. Das, P. Dubsky, A. van den Berg, and J. C. T. Eijkel, Physical Review Letters **108**, 138101 (2012).
[66] V. V. Vasilevskaya, A. A. Aerov, and A. R. Khokhlov, Journal Of Chemical Physics **120**, 9321 (2004).
[67] S. A. Allison and D. Stigter, Biophysical Journal **78**, 121 (2000).
[68] P. P. Lele, M. Mittal, and E. M. Furst, Langmuir **24**, 12842 (2008).
[69] H. Isambert, A. Ajdari, J.-L. Viovy, and J. Prost, Physical Review Letters **78**, 971 (1997).
[70] D. J. Bennett, B. Khusid, C. D. James, P. C. Galambos, M. Okandan, D. Jacqmin, and A. Acrivos, Applied Physics Letters **83**, 4866 (2003).
[71] F. Brochard and P. G. de Gennes, Journal of Chemical Physics **67**, 52 (1977).
[72] O. B. Bakajin, T. A. J. Duke, C. F. Chou, S. S. Chan, R. H. Austin, and E. C. Cox, Physical Review Letters **80**, 2737 (1998).